2023-04-01

Post-fire compressive stressstrain behaviour of steel fibre reinforced recycled aggregate concrete

Wang, T

10.1016/j.compstruct.2023.116735
Composite Structures
Elsevier

This paper is published on:
Composite Structures, *309*, 116735. doi:10.1016/j.compstruct.2023.116735

Post-fire compressive stress–strain behaviour of steel fibre reinforced recycled aggregate concrete

Tan Wang [a], Min Yu[a,b,*], Wentao Shan [a], Lihua Xu[a], ShanShan Cheng[b], Long-yuan Li[b]

a. School of Civil Engineering, Wuhan University, Wuhan 430072, China

b. School of Engineering, Computing and Mathematics, University of Plymouth, PL4 8AA, UK

Abstract: The uniaxial compressive tests were carried out to investigate the post-fire compressive stress–strain behaviour of steel fibre reinforced recycled aggregate concrete (SFR-RAC) after being exposed to elevated temperatures. The test parameters include water-to-cement ratio, recycled concrete aggregate (RCA) substituting ratio, steel fibre content and heated temperature. The failure mode, strength, elastic modulus, peak strain, and strain-stress response of the tested specimens are analysed. The test results show that the compressive strength and elastic modulus decreased with the increase of water-to-cement ratio and/or RCA substituting ratio at any exposed temperature. The residual strength retained about 83%, 85%, 56% and 23% of their ambient compressive strength on average after being exposed to 20, 400, 600 and 800°C, respectively. The steel fibre has a positive effect on the residual mechanical properties and its effect increases with the increase of heated temperature. Based on the test data, a hand calculation method was proposed for predicting the compressive strength, peak strain, elastic modulus, and uniaxial compressive stress–strain constitutive model of the SFR-RAC.

Keywords： Recycled concrete aggregate; Steel fibre; Elevated temperatures; Residual strength; Stress-strain relationship

Nomenclature

$f_{ck,0}$, $f_{ck,r,0}$	The prism axial compression strength of normal and recycled aggregate concrete at ambient temperature
$f_{ck,T}$, $f_{ck,r,T}$	The prism axial compression strength of normal and recycled aggregate concrete at elevated temperature T
$E_{c,r,T}$	Elastic modulus of recycled aggregate concrete at elevated temperature T
$E_{c,0}$	Elastic modulus of normal concrete at ambient temperature
$\varepsilon_{r,T}$	Peak strain of recycled aggregate concrete at elevated temperature T
ε_0	Peak strain of normal concrete at room temperature
S	Steel fibre content
W	Water-to-cement ratio
R	Recycled concrete aggregate substituting ratio

1 Introduction

Infrastructure construction requires a large amount of non-renewable natural resources such as sand and stone to be exploited. At the same time, a large amount of construction waste from the demolition of old structures is transported to the suburbs for stacking or landfill in the traditional way, which not only requires a lot of freight, but also causes secondary pollution to the environment. Recycling and reusing the construction and demolition wastes is a promising approach to resolve both the resource consumption and environment pollution issues. In recent years more and more recycled concrete aggregate (RCA) has been used as the replacement of natural aggregate (NA). Compared to NA, RCA has some drawbacks such as high water absorption, large porosity, and low strength, which inevitably restricts its wide application in construction industry[1-6].

To overcome the drawbacks of RCA, various techniques have been used to improve the physical properties of RCA. Examples include the pre-soaking in acid[7], two-stage mixing approach (TSMA)[8], addition of pozzolanic micro-powders[9], use of polymer emulsion[10], microbial carbonate bio-deposition[11], carbonation[12], and fibre enhancement[13-15]. Steel fibre enhancement is one of the most effective enhancement methods for improving the properties of recycled aggregate concrete (RAC), which can significantly reduce the mortar shrinkage and delay crack initiation and propagation, resulting in the improvement of strength and energy absorption capacity of RAC. There are many studies on the fibre enhancement on RAC and the applications of steel fibre reinforced recycled aggregate concrete (SFR-RAC) [16-19]. These studies have demonstrated that there is a great potential to use the SFR-RAC in construction industry in meeting the sustainability demands.

During the service life of RAC, typically 50 or 100 years, fire risk is inevitable. When a structure is subjected to a fire accident, the mechanical properties of concrete, such as its strength and elastic modulus, will inevitably degrade under the heating and the cooling after heating. Extensive research has been carried out to investigate the post-fire behaviour of different types of concrete including NAC with steel fibre and RAC without steel fibre [20-24]. However, few studies have focused on SFR-RAC subjected to high temperatures. Gao pointed out that the steel fibre has better reinforcing effect on RAC compared with NAC[25], and thus the research on the post-fire mechanical properties of steel fibre reinforced NAC (SFR-NAC) cannot be directly used for SFR-RAC. In view of fire-resistance design, the post-fire mechanical properties of SFR-RAC should be fully investigated before the material is used in structures. In this paper we present an experimental study on the post-fire residual stress–strain behaviour of SFR-RAC subjected to axial compression. The test parameters include the water-to-cement ratio, RCA substituting ratio, steel fibre volume fraction, and heated temperature. Based on the test data, a hand calculation method is proposed for calculating the residual compressive strength, peak strain, elastic modulus, and uniaxial compression stress–strain constitutive model.

2 Experimental program

2.1 Raw material and mix design

The raw materials used for concrete mixtures include the P.O42.5 cement, water, river sand, steel fibre, plasticizer, NA, and RCA. The river sand used is the class II sand specified in standard GB/T 14684–2011 with fineness modulus of 2.7. The particle sizes of NA and RCA (as shown in Fig. 1) range from 5mm to 20mm, and their grading complies with the requirements of ASTM C33. The physical performance indexes of NA and RCA are listed in Table 1. The steel fibre was a single hook end fibre with 30 mm in length and 0.75 mm in diameter, which has a tensile strength of 1250 MPa. The polycarboxylate superplasticizer with the water reduction of 0.2 was used to increase the workability of the fresh concrete.

Table 1 Physical performance indexes of aggregate

Aggregate type	Apparent density (kg/m^3)	Packing density (kg/m^3)	Crushing index (%)	Water absorption (%)
Natural aggregate (NA)	2615	1634	15	1.75
Recycled concrete aggregate (RCA)	2413	1475	18	4.87

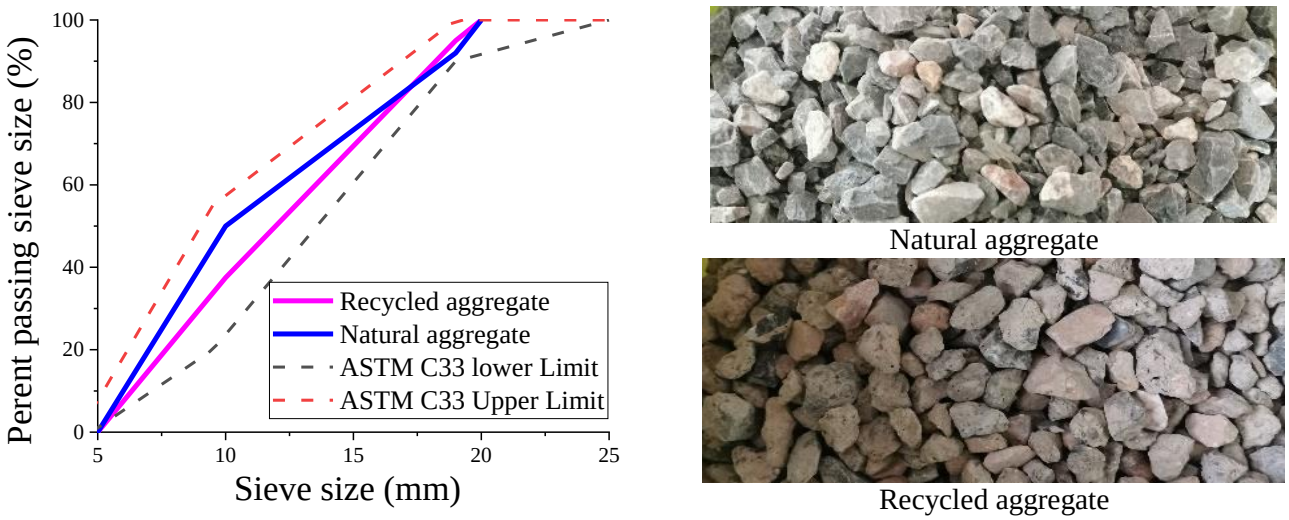

Fig. 1 Particle size distribution curve of aggregates and their appearance

Parameters such as the water-to-cement ratio, RCA substitution ratio, and volume fraction of steel fibre were selected as the main research parameters. More specifically, two volume fractions of steel fibre (S= 0% and 2%), five levels of RCA substituting ratio (0%, 30%, 50%, 70% and 100%), and three levels of water-to-cement ratio (0.35, 0.4 and 0.47) were selected in the present study. For the convenience of documenting specimens, the mix was labelled as '*SxxRyyWzz*', in which 'S' denotes the steel fibre and '*xx*' refers to the volume fraction, '*R*' represents the RCA substituting ratio and '*yy*' is the corresponding substituting ratio, 'W' represents the water-to-cement ratio and '*zz*' indicates the corresponding ratio. The

details of the mix are summarized in Table 2. All concrete mixes were designed to be exposed to five levels of temperature (20℃, 200℃, 400℃, 600℃, and 800℃). In total 50 groups of prisms specimens with the size of 150 × 150 × 300 mm were prepared for the axial compression test, and the size meets the requirements of the Chinese standard CECS13-2009[26].

Table 2 Mix proportions of concrete (units: kg/m^3)

Mix ID	Component					Water/cement Ratio (W)	RCA substitution ratio (R)	Volume fraction of steel fibre (S)
	Water	Cement	Fine aggregate	Coarse aggregate	Plasticizer			
S15R50W40	180	450	637	1133	6.3	0.4	50%	1.5%
S15R50W47	172	363	674	1191	5.08	0.47	50%	1.5%
S15R50W35	155	470	681	1114	6.58	0.35	50%	1.5%
S00R50W40	180	450	637	1133	6.3	0.4	50%	0%
S10R50W40	180	450	637	1133	6.3	0.4	50%	1%
S20R50W40	180	450	637	1133	6.3	0.4	50%	2%
S15R00W40	180	450	637	1133	6.3	0.4	0%	1.5%
S15R30W40	180	450	637	1133	6.3	0.4	30%	1.5%
S15R70W40	180	450	637	1133	6.3	0.4	70%	1.5%
S15R100W40	180	450	637	1133	6.3	0.4	100%	1.5%

2.2 Preparation and curing of specimens

As shown in Fig. 2, all dry materials (e.g. RCA, NA, river sand, steel fibre, and cement) were first put into the horizontal-shaft forced concrete mixer and the mix time were set to be one minute; the water and plasticizer were then poured into the mixer and mixed for a further five minutes; after mixing, the fresh concrete was cast into plastic moulds and vibrated for one minute. After casting, all specimens were stored at room temperature for 24 hours before demoulding, then the specimens were moved to the curing room with the relative humidity of over 90% for 90 days, where the specimens were covered by a hemp bag to keep the required relative humidity. To avoid the possible effect of high humidity on concrete strength, the specimens were moved to a well-ventilated place afterwards for another 28 days before testing[22].

Fig. 2 The process of fabrication of tested specimens

2.3 High temperature treatment and mechanical tests

The specimens were heated in an electric furnace with constant rate of 3 ℃/min until the target

temperature. After reaching the target temperature, the furnace temperature was held for 3 hours to obtain a relatively uniform temperature field within the specimens. The specimens were then moved to the physical and mechanical testing laboratories for characterization after the temperature reduced to the room temperature.

Before the mechanical testing, both ends of the heated specimens were polished to create flat surfaces. The front surface of the specimens was then sprayed with speckles for monitoring the deformation using Digital image correlation (DIC) method. The axial compression tests were carried out using MTS loading system with a maximum load capacity of 2500kN (as show in Fig. 3). A pre-load of ~30% of the peak load was applied to the specimens to remove any tolerance gaps in the machine. During the tests the specimens were first loaded to 70% of the peak load with stress rate of 0.8 MPa/s, and then loaded at an axial strain rate of 0.0012/s, and finally terminated as the load drops to 20% of the peak load.

a) Furnace

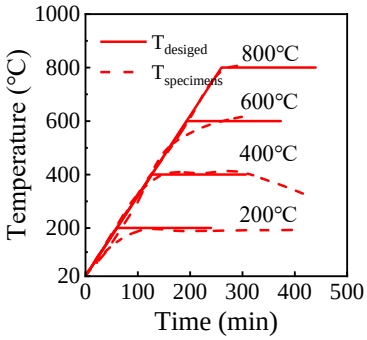

b) Temperature curves

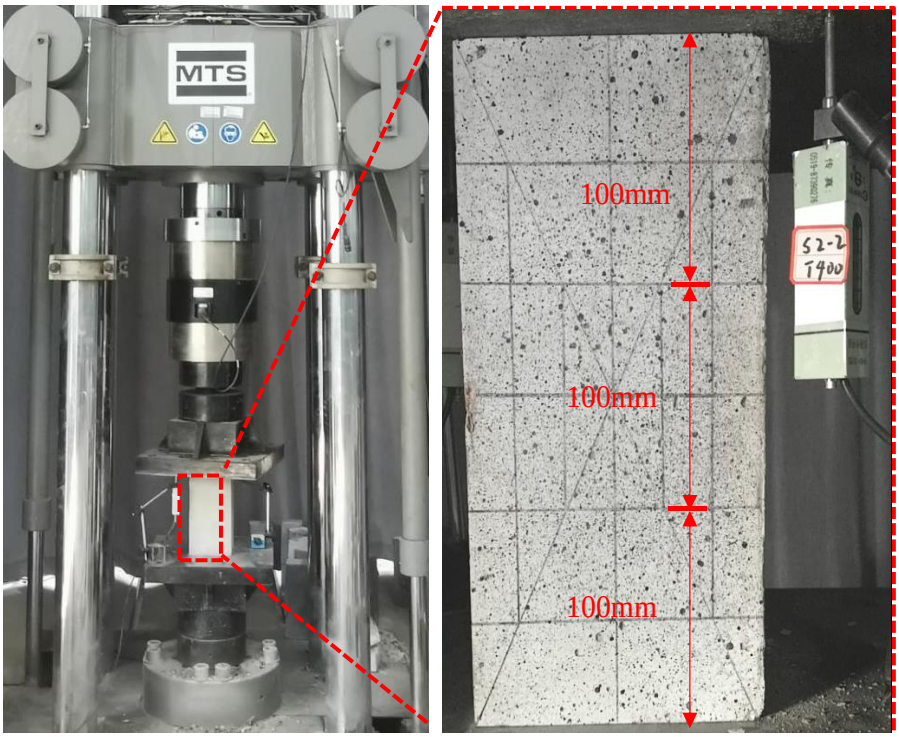

c) Test equipment and measurement methods

Fig. 3 Heating and loading processes

3 Test results and analysis

3.1 Failure mode

It is well known that, when a plain concrete prism is subjected to an axial compression its failure mode could be the shear failure, or lateral splitting failure, or the combination of shear and splitting failure, depending on the aspect ratio of the prismatic specimen. The typical failure modes of the specimens tested in the present study are presented in Fig. 4, in which the subfigure corresponds to the specimens having different water-to-cement ratios, different aggregate replacement ratios, and different steel fibre volume fractions, respectively. It can be observed from the figure that, all of the failure modes except for the

specimen of S=2% and 800 ºC are the shear failure. In the former a few of large incline cracks are very evident; whereas in the latter the specimen has a large number of no particularly orientated small cracks. This indicates that both the water-to-cement ratio and aggregate substituting ratio have nearly no influence on the failure mode. The steel fibre may have some effect on the failure mode but only when the specimen has large steel fibre volume fraction and had very high temperature exposure. The failure mode change of the specimen with large steel fibre volume fraction after a high temperature exposure is probably due to the severe material damage developed at the interface between the concrete and steel fibres at the high temperature, which leads to the specimen to have a large number of weak-links and results in a "plastic-type" failure when it is under the axial compression.

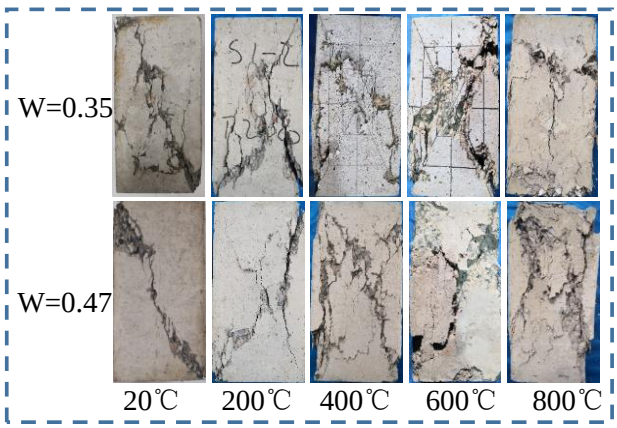

a) Influence of water-to-cement ratio

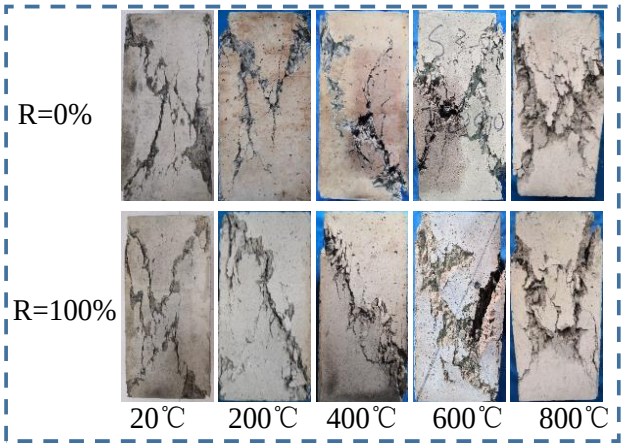

b) Influence of aggregate substituting ratio

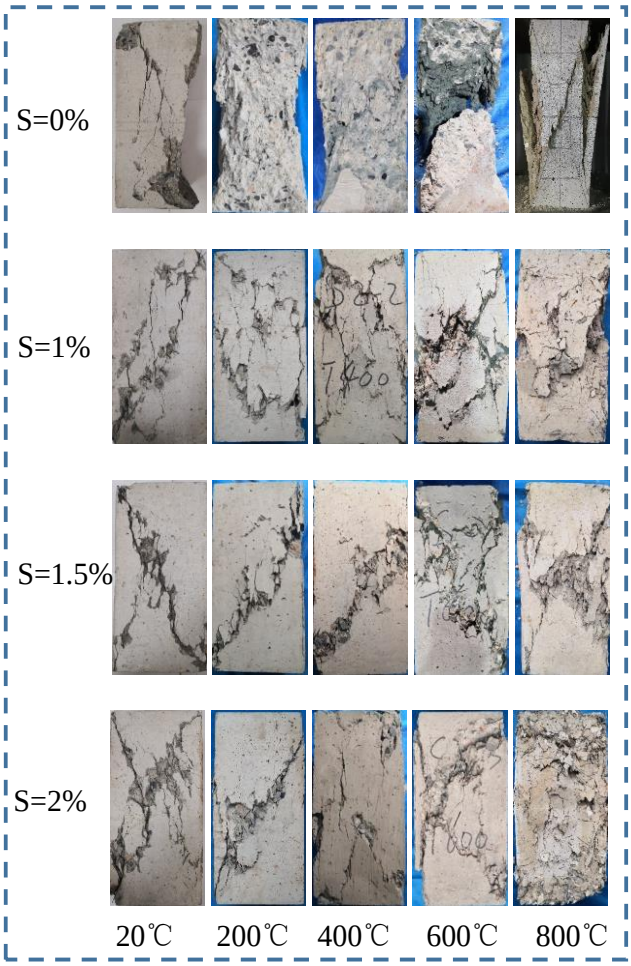

c) Influence of steel fibre

Fig. 4 Typical failure modes of tested specimens

3.2 Stress-strain curves

The stress-strain curves of all tested specimens are shown in Fig. 5, in which the dotted lines are the calculation result of theoretical model according to the formula, which will be discussed and reported in Section 4. The differences in the stress-strain curves between the specimens with different mixes can be also found in Fig. 5. Generally, the ascending part of the stress–strain curves become less stiff when the exposed temperature becomes higher due to the decrease of both the compressive strength and elastic modulus after exposed to elevated temperatures. The descending part of the stress-strain curves becomes

less brittle when the exposed temperature increases because of the formation of thermal cracks at high temperature environment.

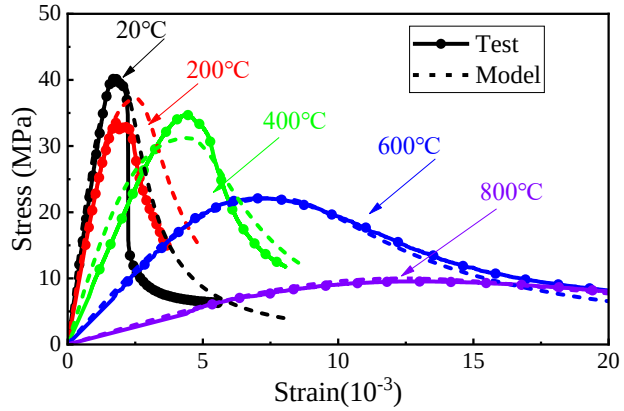

a) S15R50W40

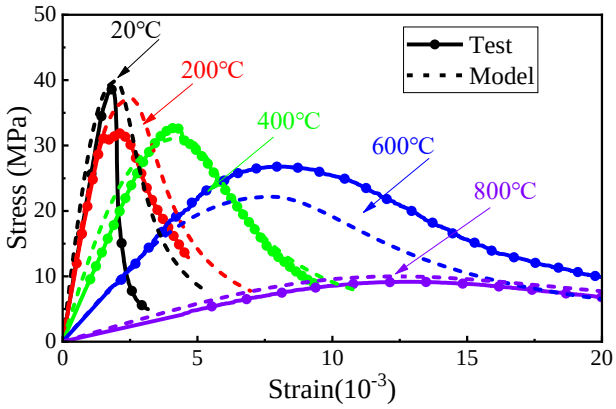

b) S15R50W47

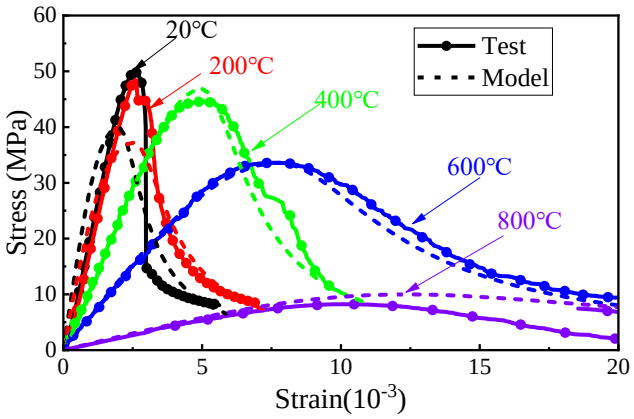

c) S15R50W35

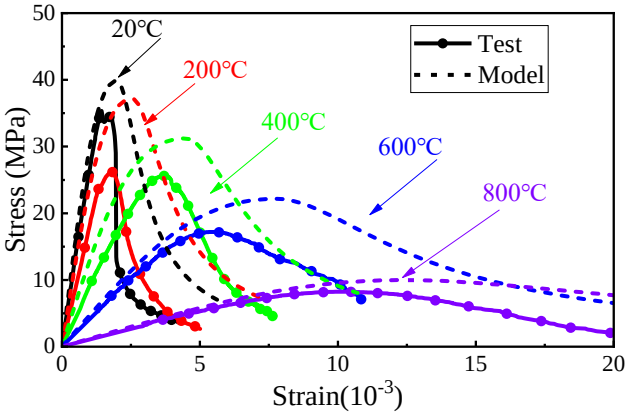

d) S00R50W40

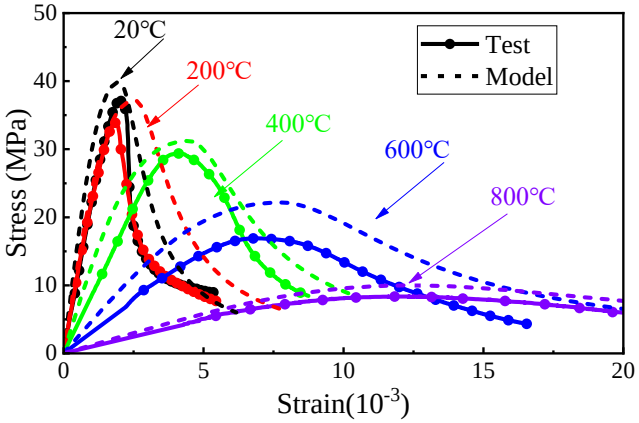

e) S10R50W40

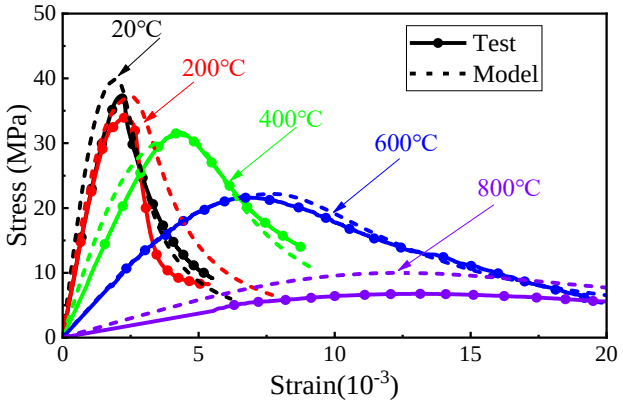

f) S20R50W40

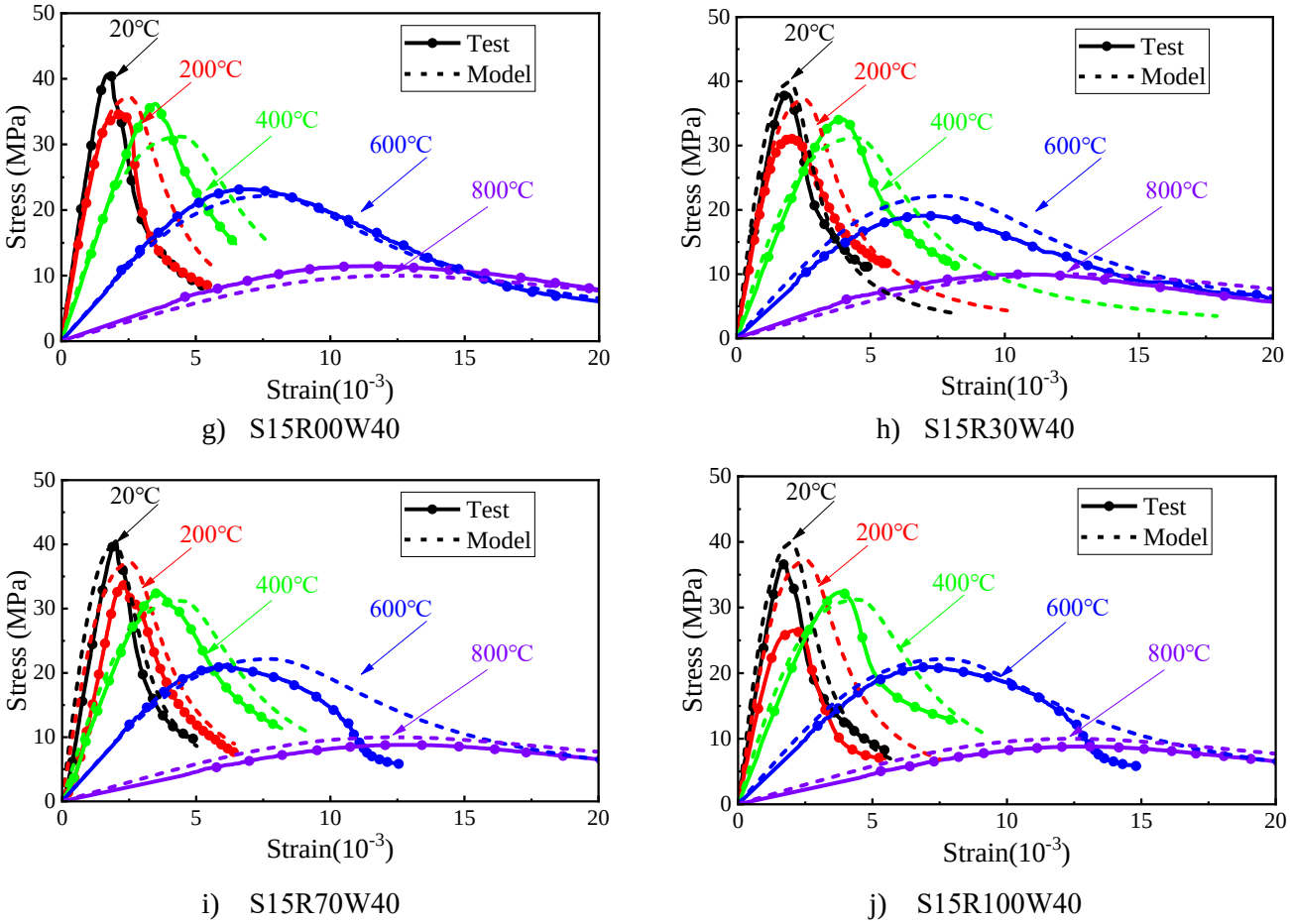

Fig. 5 Comparison between the stress–strain curves from experiments and the proposed model

The general trend of the stress-strain curves could be described as shown in Fig. 6, which includes four stages: elastic stage (OA), elastoplastic stage (AB), post-ultimate declining stage (BC), and failure stage (CD). At the elastic stage, the stress increased almost linearly with the increase of strain and there was no obvious cracking found on the surface of the specimens. As the stress exceeded approximately 70% of the ultimate strength, the curve entered the elastoplastic stage, where micro-cracks were developed. In this stage steel fibres started to play an enhanced role in suppressing the crack development. After the stress reached to the peak value, the curve entered the declining stage, where the micro-cracks widened up and became visible to naked eye. In this stage, the specimens that have higher steel fibre content (e.g., 1.5%) have higher resistance to the development of cracks. As the curve reached to the convergence point *C*, the curve entered the failure stage. A fracture zone started to appear following the shear plane and the width of the fracture zone gradually increased.

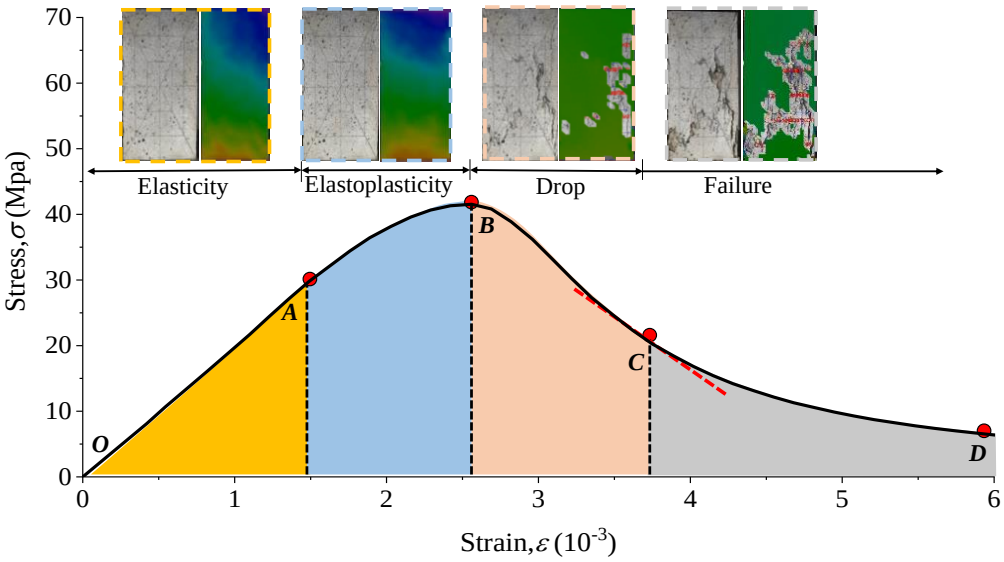

Fig. 6 The typical axial compression stress-strain curve

3.3 Compressive strength

Fig. 7 shows the individual effects of water-to-cement ratio, RCA substitution ratio, and steel fibre volume fraction on the compressive strength after different temperatures. In general, the strength decreases with the increase of water-to-cement ratio and the RCA substitution ratio, and the addition of steel fibre improves the strength of RAC until an optimum volume fraction ratio of 1.5%, after which the strength reduces with further increase of steel fibre due to balling effect. The reduction of the compressive strength due to RCA replacement can be attributed to weak ITZ and possible microcracks in the RCA[27]. It is interesting to notice that, after the high temperature exposure (800 °C) the effect of water-to-cement ratio, RCA substitution ratio, and steel fibre volume fraction on the residual compressive strength all becomes very small. The reason for this is because the damage developed at the high temperature is far more than the defects existed in the specimens when different mixes were used.

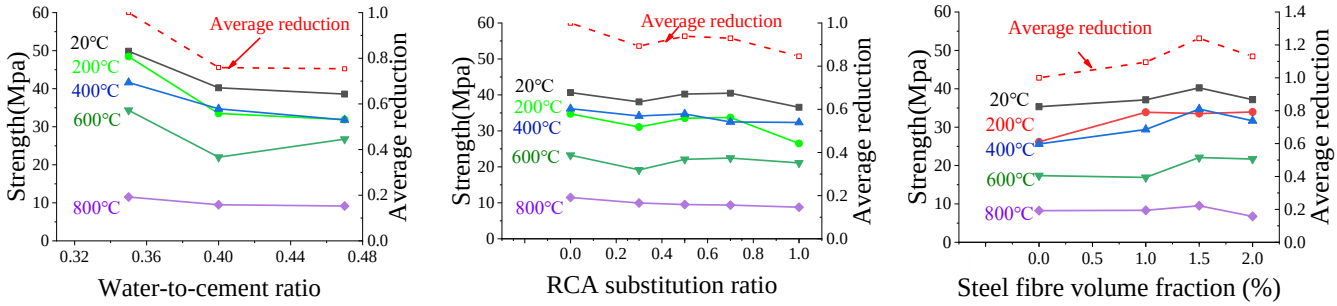

a) Water-to-cement ratio b) RCA substitution ratio c) Steel fibre volume fraction

Fig. 7 The influence of individual parameters on compressive strength after different temperature exposures

The relationship between the compressive strength and temperature of all specimens are plotted in Fig. 8, in which the curves are the average value of the specimens corresponding to the heated temperature. Overall, the compressive strength decreases with the increase of temperature. The reduction law of strength can be divided into three stages according to heated temperatures: 20~200℃, 200~400℃, and 400~800℃. When the heated temperature is lower than 200℃, a considerable reduction of strength could be found.

However, the reduction slows down when the heated temperature is between 200 and 400℃. When the temperature is beyond 400℃, a significant decrease can be found. Generally, the residual properties of RAC are undesirably affected at elevated temperatures[28]. The exposure of RAC to elevated temperature results in several physical and chemical alteration. Before 200℃, the evaporation of capillary water induces significant internal stresses on the solid skeleton and causes the reduction of strength. Another possible explanation is that the reduction of the cohesive forces between the C-S-H gel layers as water expands[29]. When the temperature is in the range of 200~400℃, hydration of unhydrated cement grains is improved due to an internal autoclaving condition as a result of the high temperature and the evaporation of water[30], which counteracts the strength reduction due to heating treatment. Meanwhile, the loss of adsorbed water and deterioration of ITZ at elevated temperatures up to 300 ℃ is the main reason for the strength loss [30]. Therefore, considering the positive and negative factors for the strength, the reduction slows down when the heated temperature is between 200 and 400℃.When the heated temperature is beyond 400℃, the hydration products of calcium hydroxide (CH) and calcium silicate hydrate (CSH) gel dehydrate and decompose, meanwhile, the siliceous aggregates transform from α -phase to β -phase causing expansion of concrete, leading to the remarkable coarsening of pore structures[31], and thus results in strength reduction.

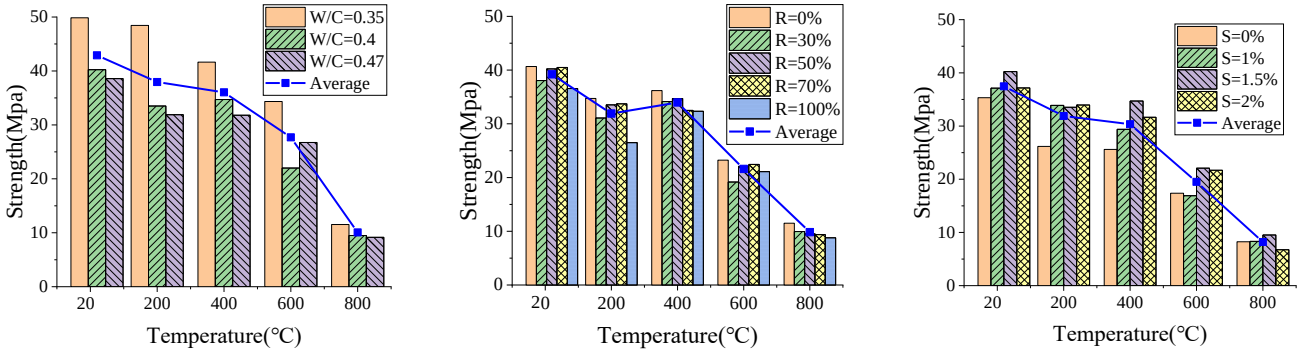

a) Water-cement ratio b) RCA substitution ratio c) Steel fibre volume fraction

Fig. 8 Compressive strength of concrete samples versus temperature

3.4 Elastic modulus

The elastic modulus was taken as the secant modulus of the stress-strain curve between 0.2-0.4 peak stress in this study. Fig. 9 presents the effects of water-to-cement ratio, RCA substitution ratio and the steel fibre volume fraction on the elastic modulus of RAC after being heated to various temperatures. It can be found that the elastic modulus generally decreases with the increase of the water-to-cement ratio and RCA substitution ratio, but increases with the increase of added steel fibre volume fraction due to the higher elastic modulus and bridge effect of steel fibres. Similar to the compressive strength, when the exposure temperatures become higher the effect of the water-to-cement ratio, RCA substitution ratio and steel fibre volume fraction on the residual elastic modulus becomes smaller and is negligible when the exposure temperature reaches 800 ℃.

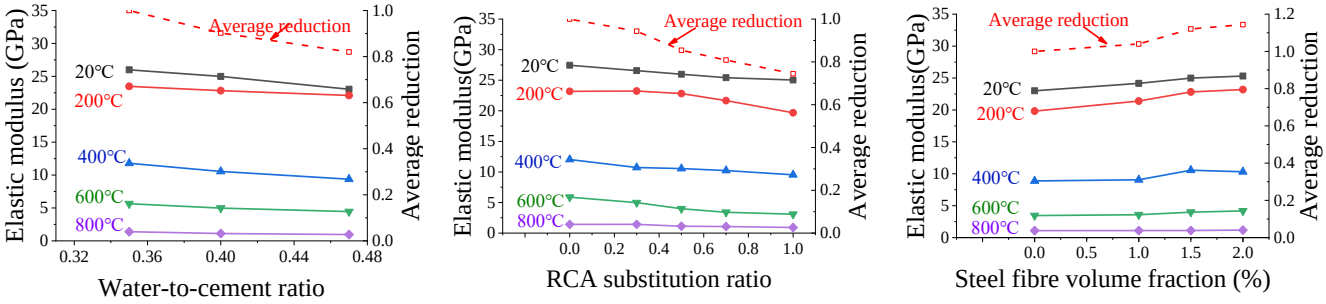

a) Water-cement ratio b) RCA substitution ratio c) Steel fibre volume fraction

Fig. 9 The influence of individual parameters on residual elastic modulus at different temperature exposures

Fig. 10 presents the elastic modulus of the specimens after being heated to various temperatures. It can be found that the elastic modulus decreased with the increase of heated temperature, regardless of the concrete mix. Moreover, from the comparison between Fig. 8 and Fig. 10, it is found that the reduction in elastic modulus is greater than the reduction in the compressive strength for the specimens subjected to the same heated temperature. There were two stages for this decrease; one is 20~200℃ and the other is 200℃~800℃. When the heated temperature is below the 200℃, the elastic modulus decreases slightly, and the average residual elastic modulus retains about 83% at 200℃. When the heated temperature is beyond 200℃, the elastic modulus decreases rapidly with the increase of heated temperature and the average residual elastic modulus retained about 39%, 12% and 3% of their unheated elastic modulus on average after being exposed to 400, 600 and 800℃.

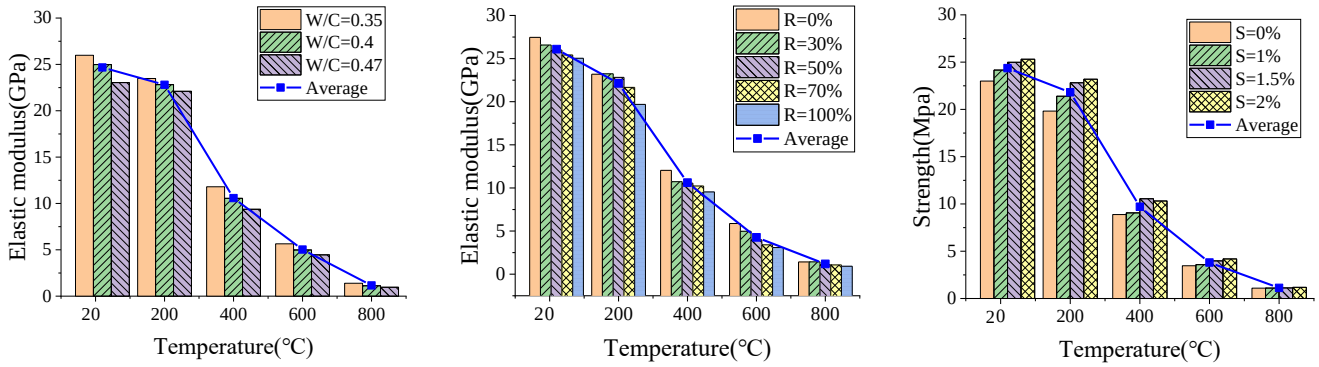

a) Water-cement ratio b) RCA substitution ratio c) Steel fibre volume fraction

Fig. 10 Elastic modulus of concrete samples versus temperature

3.5 Peak strain

The peak strain refers to the strain corresponding to the peak stress of a specimen, which is one index reflecting the deformation capacity of concrete. Fig. 11 presents the influence of water-to-cement ratio, RCA substitution ratio, and steel fibre volume fraction on the peak strain. It can be found that the peak strain generally decreases with the increase of the water-to-cement ratio, but increases with the increase of either RCA substitution ratio or steel fibre volume fraction. The increase of peak strain due to RCA can be attributed to both the low elastic modulus of RCA compared with NA, and the high porosity of attached

mortar and ITZs[32,33]. The increase of peak strain with the addition of steel fibres is due to the restriction of the widening up of microcracks, which makes concrete less brittle.

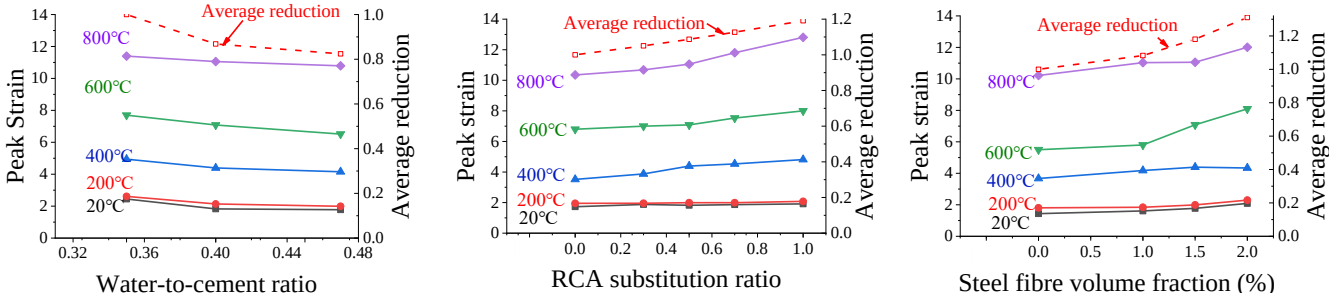

a) Water-to-cement ratio b) RCA substitution ratio c) Steel fibre volume fraction

Fig. 11 The influence of the research parameters on the peak strain at different temperature

Fig. 12 shows the peak strain of specimens versus temperature. It can be seen that the peak strain gradually increased with the increase of the heated temperature regardless of the concrete mix proportions. Similar to the elastic modulus, there were two stages for this increase: 20–200℃ and 200℃–800℃. When the heated temperature is below 200℃, the peak strain does not change significantly and the peak strain of the specimen after being exposed to 200℃ is 1.1 times of that of unheated specimens. However, when the heated temperature is beyond 200℃, there is a rapid growth and the post-fire peak strain of the specimens after being exposed to 400, 600 and 800℃ are 2.2, 4.3, and 5.2 times on average of that of unheated specimens, respectively. Generally, the peak strain is correlated positively with the strength and negatively with the elastic modulus. That is, the higher the peak strain, the higher the compressive strength but the smaller the elastic modulus.

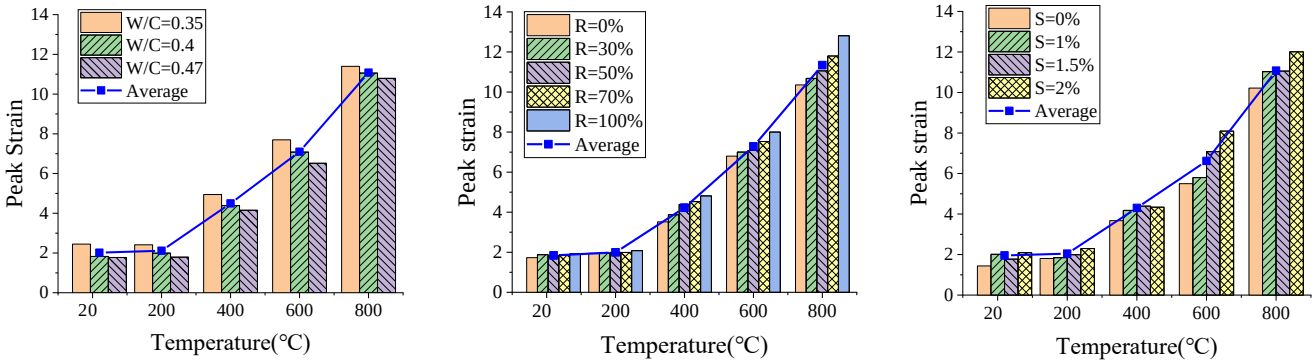

a) Water-to-cement ratio b) RCA substitution ratio c) Steel fibre volume fraction

Fig. 12 Peak strain of concrete samples versus temperature

4 Unified calculation of post-fire residual stress–strain relations

4.1 Calculation of residual strength, elastic modulus, and peak strain

Inspired by the previous research on stress-strain relations of steel fibre reinforced concrete[25], the unified formulae of post-fire residual compressive strength ($f_{ck,r,T}$), elastic modulus ($E_{c,r,T}$) and peak strain

($\varepsilon_{c,r,T}$) are proposed by modifying the compressive strength ($f_{ck,0}$), elastic modulus ($E_{c,0}$) and peak strain ($\varepsilon_{c,0}$) of normal concrete at room temperature:

$$f_{ck,r,T} = f_{ck,0} \cdot k_{f,s} \cdot k_{f,R} \cdot k_{f,T} \tag{1}$$

$$E_{c,r,T} = E_{c,0} \cdot k_{E,s} \cdot k_{E,R} \cdot k_{E,T} \tag{2}$$

$$\varepsilon_{c,r,T} = \varepsilon_{c,0} \cdot k_{\varepsilon,s} \cdot k_{\varepsilon,R} \cdot k_{\varepsilon,T} \tag{3}$$

As for the compressive strength ($f_{ck,0}$), elastic modulus ($E_{c,0}$) and peak strain ($\varepsilon_{c,0}$) of normal concrete at room temperature, Chinese code JGJ 55-2011[34] states the relationship between water-to-cement ratio (W) and compressive strength ($f_{ck,0}$) for normal concrete at room temperature, and the Chinese code GB50010[35] provides the relationship of elastic modulus ($E_{c,0}$) and peak strain ($\varepsilon_{c,0}$) with the compressive strength for normal concrete at room temperature, as follows

$$f_{ck,0} = (\alpha_a f_b / W - \alpha_a \alpha_b f_b)\beta_1\beta_2 \tag{4}$$

$$E_{c,\,0} = \frac{10^5}{2.2 + 34.7/f_{ck,0}} \tag{5}$$

$$\varepsilon_{c,0} = (700 + 172\sqrt{f_{ck,0}}) \times 10^{-6} \tag{6}$$

where α_a and α_b are the regression coefficients related to the coarse aggregate type ($\alpha_a = 0.53$ and $\alpha_b = 0.2$ for crushed stone); f_b is the compressive strength of the cement, which is $49.3MPa$ for P.O42.5 cement; $\beta_1 = f_{ck,0}/f_{cu,0} = 0.724$ is obtained by fitting test data. β_2 is the parameter related to the other factors affecting the strength of the concrete such as pouring process and material quantities, which is taken as $\beta_2 = 1$ in this study.

Moreover, as stated in Section 3, all the testing parameters (steel fibre, RCA substituting ratio and temperature) have significant influence on the stress-strain constitutive relation such as the compressive strength, elastic modulus and peak strain. The influence factors are obtained by regressing test data, which are presented in Fig. 13 and

Table 3. It should be noted the reduction of tested data in Fig.13 is the average data considering all the heated temperatures.

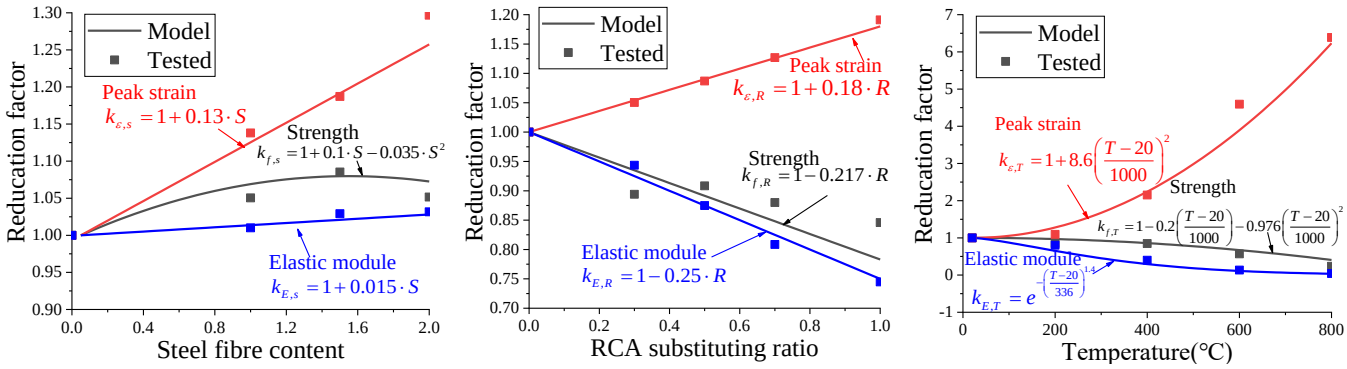

a) Steel fibre b) RCA substituting ratio c) Temperature

Fig. 13 The influence of parameter on the index

Table 3 Unified formulue of post-fire residual strength and peak strain

Index	Rectification Formula	
Strength	$k_{f,S}=1+0.1\cdot S-0.035\cdot S^2$ $k_{f,R}=1-0.217\cdot R$ $k_{f,T}=1-0.2\left(\frac{T-20}{1000}\right)-0.976\left(\frac{T-20}{1000}\right)^2$	(7)
Elastic modulus	$k_{E,S}=1+0.015\cdot S$ $k_{E,R}=1-0.25\cdot R$ $k_{E,T}=e^{-\left(\frac{T-20}{336}\right)^{1.4}}$	(8)
Peak strain	$k_{\varepsilon,S}=1+0.13\cdot S$ $k_{\varepsilon,R}=1+0.18\cdot R$ $k_{\varepsilon,T}=1+8.6\left(\frac{T-20}{1000}\right)^2$	(9)

4.2 Proposed stress–strain relations

In previous research [36-38], several analytical models have been proposed to interpret the experimental stress–strain curves. Chinese code (GB50010[35]) provides the stress–strain relations, as shown in Eq. (7), which is of good compatibility and has been successfully applied to different kinds of concrete at room temperature or elevated temperatures[39-41].

$$\sigma=\begin{cases}\dfrac{\rho_{c,r,T}n}{n-1+x^n}E_{c,r,T}\varepsilon & ,x,,1\\ \dfrac{\rho_{c,r,T}}{\alpha_{c,r,T}(x-1)^2+x}E_c\varepsilon & ,x>1\end{cases},\quad n=\frac{E_{c,r,T}\varepsilon_{c,r,T}}{E_{c,r,T}\varepsilon_{c,r,T}-f_{c,r,T}},\quad \rho_{c,r,T}=\frac{f_{c,r,T}}{E_{c,r,T}\varepsilon_{c,r,T}} \tag{10}$$

where $x=\varepsilon/\varepsilon_0$, with ε and ε_0 representing the compressive strain and the peak strain, respectively; σ and f_0 represent the compressive stress and the peak stress, respectively; $E_{c,r,T}$ is the elastic modulus; $\alpha_{c,r,T}$ is an independent factor that controls the shape of the descending curve.

In this study, the ascending phase of curve ($x \le 1$) of the Chinese code (GB50010[35]) was directly adopted. However, the descending phase of curve ($x>1$) has been modified. Fig. 14 a) presents the comparison of descending parameters $\alpha_{c,r,T}$ between the fitting results and Chinese code. It can be found that the $\alpha_{c,r,T}$ in this study is relatively bigger than the code. Meanwhile, according to GB50010, $\alpha_c<0$ when the strength is less than 10 MPa, indicating that the curve ascent after the peak stress, which is unreasonable. This may be because that the formula in GB50010 only considers the concrete at room temperature. To describe the descending trend of the post-fire concrete, the formula in GB50010 were adjusted in the present study by considering the elevated temperatures, which are presented in Fig. 14 and Eq.(8). It can be found that $\alpha_{c,r,T}>0$ in the modified formula even for low strength concrete.

$$\alpha_{c,r,T} = 0.314 f_{ck,r,T}^{0.785}(1 - 20S) \tag{11}$$

In order to illustrate the difference of the stress-strain curves between SFR-RAC after being exposed to an elevated temperature and normal concrete at room temperature, Fig. 14 b-c) compared the normalized stress-strain of the proposed model with different volume fraction of steel fibres at room temperature and different heated temperature (take 0% steel fibre as an example) with the model in Chinese code of normal concrete at room temperature. It can be seen that the descending curve of the proposed model is steeper than that of Chinese code at room temperature, and the descending curve of the proposed model becomes flatter with the increase of heated temperature and the increase of steel fibres.

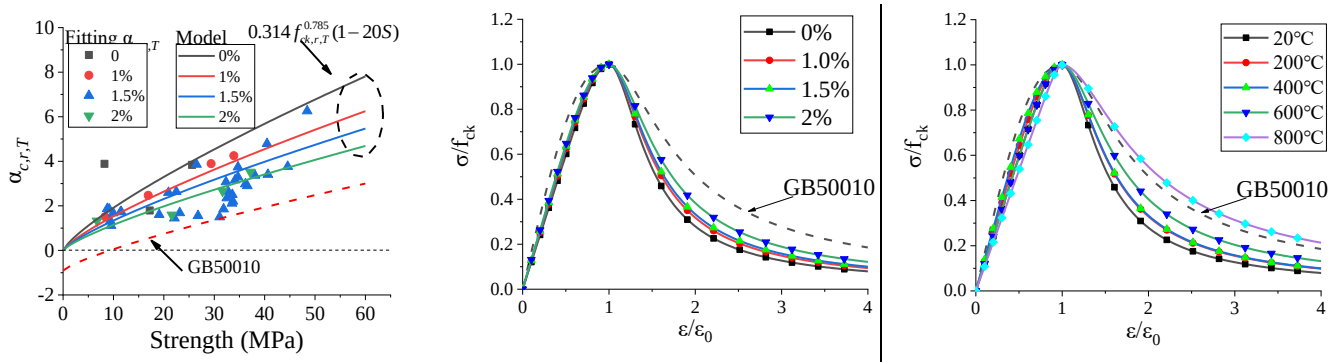

a) The descending parameters $\alpha_{c,r,T}$

b) Normalized stress-strain with different steel fibre

c) Normalized stress-strain of different temperature

Fig. 14 Comparison of descending phase of the curve between the proposed model and GB50010

4.3 Validation of the formula

Fig. 15 presents the comparison of the compressive strength and peak strain results obtained from experiments and the proposed unified model listed in

Table 3. The test results were in good agreement with the predicted values, which indicates that all the post-fire compressive strength, elastic modulus and peak strain could be predicted by the unified formulae considering the heated temperature, water-cement ratio, steel fibre volume fraction and RCA substituting ratio.

The stress–strain curves obtained from experiments and the proposed model are compared in Fig. 5. It can be found that the proposed stress-strain model agrees well with the test results considering exposure temperature, water-to-cement ratio, steel fibre volume fraction and RCA substituting ratio.

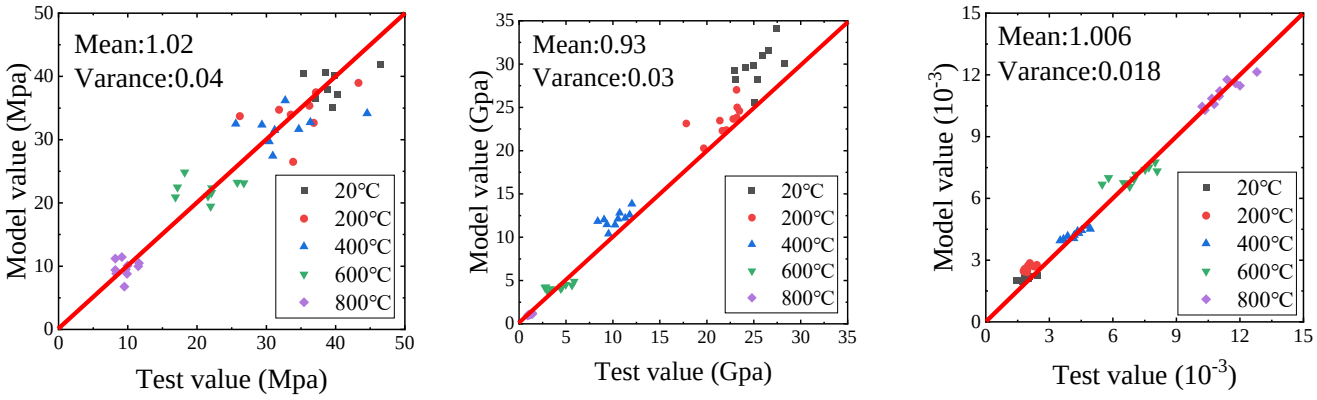

a) Compressive strength b) Elastic modulus c) Peak strain

Fig. 15 Comparison of experiment results and the proposed model results

The 15 specimens from Zhao[42] were selected to further validate the proposed unified formula. As stated in Zhao[42], the water-to-cement ratio is 0.45, the cement belongs to P.O42.5 cement, and the coarse aggregate is the crushed stone, thus $\alpha_a = 0.53$, $\alpha_b = 0.2$, and $f_b = 49.3MPa$. Moreover, the β_2 is taken as 1.2 according to the compressive strength at room temperature.

The predicted compressive strength, elastic modulus, peak strain (using the formulae listed in Table 3) and the stress-strain relationship (Eq.(7)), of the specimens from Zhao[42], were obtained and compared with the tested data in Fig.16 and Fig.17. Note that the temperature reduction factor ($k_{f,T}$ in Table 3) is taken from Zhao[42], and the relative compressive strength from Zhao is smaller than that of this study due to different raw materials used for the specimens.

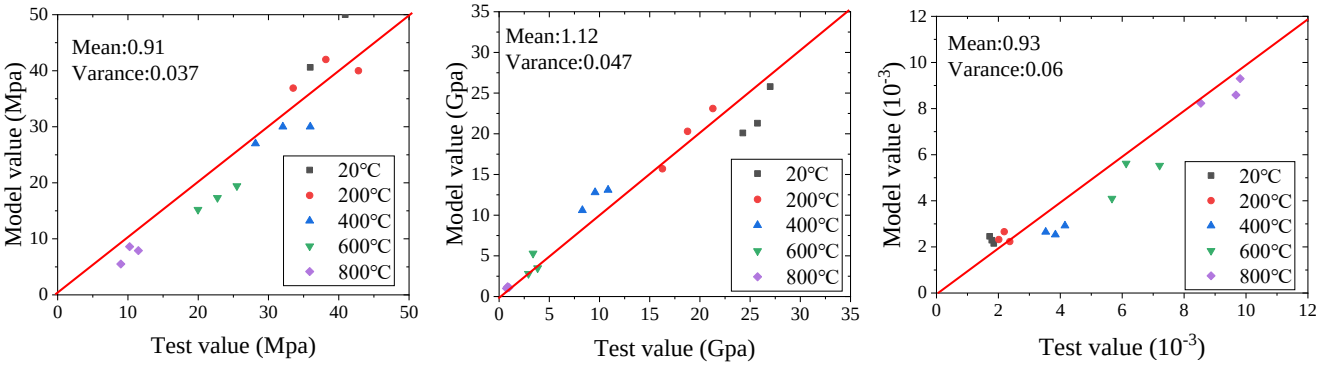

a) Compressive strength b) Elastic modulus c) Peak strain

Fig. 16 Validation of the compressive strength, elastic modulus and peak strain

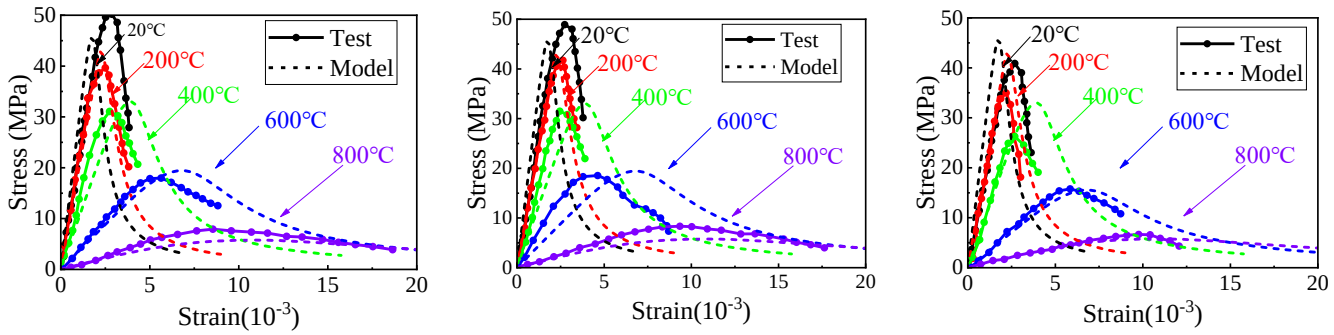

a) RCA-0 b) RCA-50 c) RCA-100

Fig. 17 Validation of the stress-strain curve

5 Conclusion

In this study, the influence of water-to-cement ratio, RCA substituting ratio and steel fibre volume fraction on the post-fire residual axial compressive behaviour of SFR-RAC were investigated. A unified formula was proposed to predict the post-fire stress-strain relationship of SFR-RAC based on the experimental data and to investigate the key influencing parameters. Based on the results obtained from this study, the following conclusions can be drawn:

1) All of the failure modes except for the specimen of S=2% and 800 ℃ are the shear failure. Both the water-to-cement ratio and RCA substituting ratio have little influence on the failure mode of the concrete at elevated temperatures, and the spalling phenomenon of the specimens with steel fibre was suppressed obviously due to the bridge effect of the steel fibres.
2) The post-fire compressive strength of RAC started to decrease under 200℃ and slightly increased between 200-400℃, and then further decreased beyond 400℃. The residual strength retained about 83%, 85%, 56% and 23% of their unheated compressive strength on average after being exposed to 20, 400, 600 and 800℃, respectively. The compressive strength generally decreased with the increase of the water-to-cement ratio or RCA substituting ratio at any expose temperature. The optimised volume fraction of steel fibres was found to be S=1.5%, where the compressive strength was the highest. However, this reinforcement effect reached its peak at 400℃ and the strength of specimens with S=1.5% steel fibres increased to 1.35 times of that of plain concrete at 400℃.
3) The elastic modulus decreased sharply after 200 ℃ and the average residual elastic modulus retained about 83%, 39%, 12% and 3% of their unheated elastic modulus on average after being exposed to 200 400, 600 and 800 ℃. With the increase of water-to-cement ratio and/or RCA substituting ratio, the elastic modulus generally decreased, but the elastic modulus increased with the increase of volume fraction of steel fibres.
4) There is a dramatical increase in the peak strain of RAC for temperatures above 200℃ regardless of the concrete mix proportions. The post-fire peak strain of the specimen after being exposed to 200, 400, 600 and 800 ℃ is 1.1, 2.2, 4.3, and 5.2 times of that of unheated specimens, respectively. The peak

strain increased with the increase of the water-to-cement ratio, the RCA substituting ratio, or the steel fibre volume fraction.

Acknowledge

This study was supported financially by the Key R&D Project of Hubei Province of China (Grant NO.2020BAB060), the National Natural Science Foundation of China (Grant NO.51878518) and H2020-MSCA-IF-2020 (Marie Skłodowska-Curie Individual Fellowships) under grant No. 101022142 (TemGPC).

References:

[1] Andreu G, Miren E. Experimental analysis of properties of high performance recycled aggregate concrete. CONSTR BUILD MATER. 2014;52：227-35.

[2] Poon CS, Shui ZH, Lam L, Fok H, Kou SC. Influence of moisture states of natural and recycled aggregates on the slump and compressive strength of concrete. CEMENT CONCRETE RES. 2004;34(1)：31-6.

[3] Duan ZH, Poon CS. Properties of recycled aggregate concrete made with recycled aggregates with different amounts of old adhered mortars. MATER DESIGN. 2014;58：19-29.

[4] Sagoe-Crentsil KK, Brown T, Taylor AH. Performance of concrete made with commercially produced coarse recycled concrete aggregate. CEMENT CONCRETE RES. 2001;31(5)：707-12.

[5] Gómez-Soberón JMV. Porosity of recycled concrete with substitution of recycled concrete aggregate: An experimental study. CEMENT CONCRETE RES. 2002;32(8)：1301-11.

[6] Cavalline TL, Weggel DC. Recycled brick masonry aggregate concrete. Structural Survey. 2013;31(3)：160-80.

[7] de Andrade Salgado F, de Andrade Silva F. Recycled aggregates from construction and demolition waste towards an application on structural concrete: A review. Journal of Building Engineering. 2022;52：104452.

[8] Tam VWY, Tam CM. Diversifying two-stage mixing approach (TSMA) for recycled aggregate concrete: TSMAs and TSMAsc. CONSTR BUILD MATER. 2008;22(10)：2068-77.

[9] Younis KH, Pilakoutas K. Strength prediction model and methods for improving recycled aggregate concrete. CONSTR BUILD MATER. 2013;49：688-701.

[10] Kou S, Poon C. Properties of concrete prepared with PVA-impregnated recycled concrete aggregates. Cement and Concrete Composites. 2010;32(8)：649-54.

[11] Qiu J, Tng DQS, Yang E. Surface treatment of recycled concrete aggregates through microbial carbonate precipitation. CONSTR BUILD MATER. 2014;57：144-50.

[12] Thiery M, Dangla P, Belin P, Habert G, Roussel N. Carbonation kinetics of a bed of recycled concrete aggregates: A laboratory study on model materials. CEMENT CONCRETE RES. 2013;46：50-65.

[13] Carneiro JA, Lima PRL, Leite MB, Toledo Filho RD. Compressive stress – strain behavior of steel fiber reinforced-recycled aggregate concrete. Cement and Concrete Composites. 2014;46：65-72.

[14] Mesbah HA, Buyle-Bodin F. Efficiency of polypropylene and metallic fibres on control of shrinkage and cracking of recycled aggregate mortars. Construction & building materials. 1999;13(8)：439-47.

[15] Erdem S, Dawson AR, Thom NH. Microstructure-linked strength properties and impact response of conventional and recycled concrete reinforced with steel and synthetic macro fibres. CONSTR BUILD MATER. 2011;25(10)：4025-36.

[16] Gao D, Li W, Pang Y, Huang Y. Behavior analysis and strength prediction of steel fiber reinforced recycled aggregate concrete column under axial compression. CONSTR BUILD MATER. 2021;290：123278.

[17] Etman EE, Afefy HM, Baraghith AT, Khedr SA. Improving the shear performance of reinforced concrete beams made of recycled coarse aggregate. CONSTR BUILD MATER. 2018;185(OCT.10)：310-24.

[18] Gao D, Zhu W, Fang D, Tang J, Zhu H. Shear behavior analysis and capacity prediction for the steel fi ber reinforced concrete beam with recycled fi ne aggregate and recycled coarse aggregate. The structural engineer. 2022(100-4).

[19] Chaboki HR, Ghalehnovi M, Karimipour A, de Brito J, Khatibinia M. RETRACTED: Shear behaviour of concrete beams with recycled aggregate and steel fibres. CONSTR BUILD MATER. 2019;204：809-27.

[20] Vieira JPB, Correia JR, de Brito J. Post-fire residual mechanical properties of concrete made with recycled concrete coarse aggregates. CEMENT CONCRETE RES. 2011;41(5)：533-41.

[21] Chen GM, He YH, Yang H, Chen JF, Guo YC. Compressive behavior of steel fiber reinforced recycled aggregate concrete after exposure to elevated temperatures. CONSTR BUILD MATER. 2014;71：1-15.

[22] Vieira JPB, Correia JR, de Brito J. Post-fire residual mechanical properties of concrete made with recycled concrete coarse aggregates. CEMENT CONCRETE RES. 2011;41(5)：533-41.

[23] Vieira JPB, Correia JR, de Brito J. Post-fire residual mechanical properties of concrete made with recycled concrete coarse aggregates. CEMENT CONCRETE RES. 2011;41(5)：533-41.

[24] Xiao J, Fan Y, Tawana MM. Residual compressive and flexural strength of a recycled aggregate concrete following elevated temperatures. STRUCT CONCRETE. 2013;14(2)：168-75.

[25] Gao D, Zhang L, Nokken M. Compressive behavior of steel fiber reinforced recycled coarse aggregate concrete designed with equivalent cubic compressive strength. CONSTR BUILD MATER. 2017;141：235-44.

[26] CECS. Standard test methods for fiber reinforced concrete. CECS 13:20092009.

[27] Fernandes B, Carré H, Mindeguia J, Perlot C, La Borderie C. Effect of elevated temperatures on concrete made with recycled concrete aggregates - An overview. Journal of Building Engineering. 2021;44：103235.

[28] Ahmed W, Lim CW, Akbar A. Influence of Elevated Temperatures on the Mechanical Performance of Sustainable-Fiber-Reinforced Recycled Aggregate Concrete: A Review. Buildings. 2022;12(4)：487.

[29] Hager I. Behaviour of cement concrete at high temperature. Bulletin of the Polish Academy of Sciences: Technical Sciences. 2013;61(1)：145-54.

[30] Babalola OE, Awoyera PO, Le DH, Bendezú Romero LM. A review of residual strength properties of normal and high strength concrete exposed to elevated temperatures: Impact of materials modification on behaviour of concrete composite. CONSTR BUILD MATER. 2021;296：123448.

[31] Lau A, Anson M. Effect of high temperatures on high performance steel fibre reinforced concrete. CEMENT CONCRETE RES. 2006;36(9)：1698-707.

[32] Liu X, Wu T, Liu Y. Stress-strain relationship for plain and fibre-reinforced lightweight aggregate concrete. CONSTR BUILD MATER. 2019;225：256-72.

[33] Xiao J, Zhang K, Akbarnezhad A. Variability of stress-strain relationship for recycled aggregate concrete under uniaxial compression loading. J CLEAN PROD. 2018;181：753-71.

[34] Wang T, Yu M, Zhang X, Cheng S, Liu S. Post-fire mechanical behaviour of ultra-high-performance concrete-filled steel tube (UHPCFST) stub columns under compression. J CONSTR STEEL RES. 2022;196：107384.

[35] Sciences CAOB. Code for design of concrete structures. GB50010. Beijing: China Architecture & Building Press, 2010.

[36] Chang YF, Chen YH, Sheu MS, Yao GC. Residual stress–strain relationship for concrete after exposure to high temperatures. CEMENT CONCRETE RES. 2006;36(10)：1999-2005.

[37] Mansur MA, Chin, Wee T TH. stress-strain relationship of high-strength fiber concrete in compression. J MATER CIVIL ENG. 1999.

[38] Zhou J, Pan J, Leung CKY. Mechanical Behavior of Fiber-Reinforced Engineered Cementitious Composites in Uniaxial Compression. J MATER CIVIL ENG. 2015;27(1)：4014111.

[39] Hua Yang HZFL, P. Compressive Stress – Strain Relationship of Concrete Containing Coarse Recycled Concrete Aggregate at Elevated Temperatures. ASCE,Journal of Materials in Civil. 2019：899-1561.

[40] Tang Y, Xiao J, Zhang H, Duan Z, Xia B. Mechanical properties and uniaxial compressive stress-strain behavior of fully

recycled aggregate concrete. CONSTR BUILD MATER. 2022;323：126546.

[41] Yan P, Wu J, Lin D, Liu X. Uniaxial compressive stress–strain relationship of mixed recycled aggregate concrete. CONSTR BUILD MATER. 2022;350：128663.

[42] Zhao H, Liu F, Yang H. Residual compressive response of concrete produced with both coarse and fine recycled concrete aggregates after thermal exposure. CONSTR BUILD MATER. 2020;244：118397.